
Information-Preserving Domain Transfer with Unlabeled Data in Misspecified Simulation-Based Inference

Joon Jang¹ Eunho Jeong² Kyu Sung Choi^{3,4,5*} Hyeonjin Kim^{3,6*}

¹Department of Biomedical Sciences, Seoul National University, Seoul, Republic of Korea

²Department of Applied Bioengineering, Graduate School of Convergence Science and Technology, Seoul National University, Seoul, Republic of Korea

³Department of Radiology, Seoul National University Hospital, Seoul, Republic of Korea

⁴Department of Radiology, Seoul National University College of Medicine, Seoul, Republic of Korea

⁵Healthcare AI Research Institute, Seoul National University Hospital, Seoul, Republic of Korea

⁶Department of Medical Sciences, Seoul National University, Seoul, Republic of Korea

Abstract

Simulation-based inference (SBI) provides amortized Bayesian parameter inference from simulator-generated data without requiring explicit likelihood evaluation. Its reliability can degrade under model misspecification, where real-world observations are not well represented by the simulator used for training. Existing methods using unlabeled real-world data often align simulated and real-world data distributions, but marginal alignment alone does not directly preserve parameter-relevant information needed for posterior inference. We propose SPIN, an SBI framework with parameter-relevant information-preserving domain transfer using unlabeled, unpaired real-world observations. During training, SPIN translates labeled simulator observations toward the real-world domain and back to the simulator domain, using the original simulator labels to encourage domain transfer that preserves parameter-relevant mutual information. At test time, the learned real-to-simulator transport maps real-world observations into the simulator domain for posterior inference, without requiring real-world parameter labels or paired real-simulator observations. Across controlled synthetic and physical real-world benchmarks, SPIN improves real-world posterior inference, with the improvement becoming clearer as misspecification increases.

1 Introduction

Simulation-based inference (SBI) is widely used for Bayesian parameter inference across scientific and engineering applications where simulators are available but explicit likelihood evaluation is inconvenient, expensive, or inaccessible [1, 2]. Modern neural SBI methods train an inference network on simulated data to learn the probabilistic relationship between simulation outputs and parameters. Neural posterior estimation (NPE), a common neural SBI approach, uses a conditional generative model to directly approximate the posterior distribution, enabling amortized inference for new observations [3, 4]. This makes NPE useful for repeated inference, but its reliability remains sensitive to *model misspecification*: when real-world observations are not well represented by the simulator, the posterior estimator is evaluated outside the distribution used for training [5, 6, 7]. Its consequences and diagnostics have been studied in approximate Bayesian computation, Bayesian asymptotics under misspecification, and neural SBI, including posterior bias, overconfidence, out-of-simulation behavior, and statistical model criticism [6, 7, 8, 9, 10, 11, 12]. In this setting, direct amortized inference on real-world data can yield biased or overconfident posteriors [7, 10, 13].

*Corresponding authors.

Recent approaches to misspecified SBI differ in the type of real-world supervision they require. RoPE [14] targets settings with a small real-world calibration set of observations with known parameters and formalizes the misspecification gap as an optimal-transport problem [15, 16, 17] between learned representations of real-world and simulated observations. FRISBI [18] extends this known-parameter real-world data setting to an inductive and amortized setting using OT-based alignment over unpaired observations.

Without such a calibration set, recent work has used unlabeled real-world observations during training. NPE with self-consistency (NPE+SC) [13] augments the simulation-based posterior loss with a self-consistency loss evaluated on unlabeled observations. This loss exploits the Bayesian self-consistency relation [19, 20] that the likelihood–prior to posterior ratio is constant across parameter values under exact inference. However, evaluating this constraint requires likelihood evaluations or an auxiliary likelihood estimator.

Other methods using unlabeled real-world data include domain alignment methods such as NPE with robust statistics (NPE-RS) [12], NPE-MMD [21], and NPE-DANN [21]. NPE-RS and NPE-MMD use maximum mean discrepancy (MMD) [22] alignment, while NPE-DANN uses domain-adversarial neural network (DANN) alignment [23]. These methods show that domain alignment with unlabeled data can improve robustness under model misspecification, but their adaptation objectives primarily match marginal summary distributions or induce domain confusion in summary space. The underlying issue is that marginal alignment does not determine the conditional structure relating observations to task variables. This limitation is closely related to results in domain adaptation, where marginal invariance does not ensure conditional invariance and non-invertible representations can lose information needed for prediction [24, 25, 26]. Similarly, translation-based domain adaptation has used semantic-consistency constraints because aligning marginal distributions does not enforce semantic consistency and may change label-relevant content [27]. Thus, marginal domain alignment is useful but only indirectly constrains the information needed for posterior inference.

We therefore propose SPIN, an SBI framework with parameter-relevant information-preserving domain transfer for NPE under model misspecification. SPIN learns bidirectional simulator–real-world transports using a variational lower-bound objective designed to preserve parameter-relevant information after transport. During training, a labeled simulator observation is translated toward the real-world domain and then mapped back to the simulator domain. Because this transported observation originates from a labeled simulator sample, the original simulator parameter label remains available, allowing SPIN to optimize the information-preserving constraint without real-world parameter labels or paired real–simulator observations. At test time, the learned real-to-simulator transport maps each real-world observation into the simulator domain before posterior evaluation. Our main contributions are as follows:

1. **Information-preserving domain transfer.** SPIN constrains domain transfer to preserve information needed for posterior inference, rather than relying only on marginal alignment between simulated and real-world data.
2. **Unlabeled, unpaired real-world adaptation.** SPIN requires only simulator labels for training, enabling NPE adaptation with unlabeled, unpaired real-world observations without real-world parameter labels.

Across synthetic and controlled physical real-world benchmarks, SPIN improves the main inference-quality metrics, with larger gains as the simulator–reality gap increases.

2 Method

2.1 Problem setup

Let $\theta \in \Theta$ denote the parameter of interest and let $x_s \in \mathcal{X}_s$ denote a simulated observation generated from $p_s(x_s | \theta)$ with prior $p(\theta)$. Let $x_r \in \mathcal{X}_r$ denote a real-world observation. We assume access to N_s labeled simulated pairs $\mathcal{D}_s = \{(\theta_i^s, x_{s,i})\}_{i=1}^{N_s}$ and N_r unlabeled real-world observations $\mathcal{D}_r = \{x_{r,j}\}_{j=1}^{N_r}$. Real-world observations are available without parameter labels and without pairing to individual simulated samples.

NPE learns a conditional density estimator from simulated parameter–observation pairs [3, 4]. This estimator is often parameterized as a conditional normalizing flow, and for high-dimensional observations it is commonly conditioned on a neural statistic estimator h_ω [28, 29]:

$$q_{\psi,\omega}(\theta | x_s) := q_\psi(\theta | h_\omega(x_s)).$$

For notational simplicity, we write $q_\psi(\theta | x)$ throughout the paper, with the understanding that this denotes $q_\psi(\theta | h_\omega(x))$ when a summary network is used. Standard NPE minimizes the negative conditional log-likelihood of simulator parameters under the posterior density estimator [3, 4]. We denote this simulator-side conditional density objective for a generic estimator q by

$$\mathcal{L}_s(q) := \mathbb{E}_{(\theta, x_s) \sim p_s(\theta, x_s)} [-\log q(\theta | x_s)].$$

Under model misspecification, direct evaluation of a simulator-trained posterior on x_r can be unreliable because real-world observations may not be represented by the simulator distribution [7, 10, 13]. SPIN therefore defines test-time inference after real-to-simulator transport:

$$\hat{p}(\theta | x_r) := q_\psi(\theta | x_{rs}), \quad x_{rs} := G_{rs}(x_r). \quad (1)$$

Here, $G_{rs} : \mathcal{X}_r \rightarrow \mathcal{X}_s$ denotes the real-to-simulator transport. We also introduce the reverse transport $G_{sr} : \mathcal{X}_s \rightarrow \mathcal{X}_r$, which maps simulator observations toward the real-world domain. The two transports define a bidirectional observation-space translation [30]: G_{sr} produces observations in the real-world domain from simulator samples, and G_{rs} maps real-world observations into the simulator domain used by the posterior estimator. For reliable test-time inference, G_{rs} should transport observations to the simulator domain while preserving parameter-relevant information.

2.2 Parameter-relevant information-preserving domain transfer

As an idealized reference, suppose that real-world parameter labels were available. Then preservation of parameter-relevant information under the test-time transport G_{rs} could be expressed by maximizing the mutual information (MI) [31, 32]:

$$\max_{G_{rs}} I_r(\Theta; G_{rs}(X_r)).$$

Here, $I_r(\cdot; \cdot)$ denotes MI under the real-world joint distribution. In the unlabeled real-world setting, this objective is not available. We therefore approach the information-maximization problem using transported simulator observations that retain their simulator labels.

For a simulated pair (θ, x_s) , define

$$x_{sr} := G_{sr}(x_s), \quad x_{srs} := G_{rs}(x_{sr}) = G_{rs}(G_{sr}(x_s)).$$

The observation x_s is first translated toward the real-world domain and then mapped back to the simulator domain. Because x_{srs} originates from a labeled simulator sample, the original simulator parameter label remains available. The information transmitted through this transported observation can be quantified by the MI

$$I_s(\Theta; G_{rs}(G_{sr}(X_s))) = H_s(\Theta) - H_s(\Theta | G_{rs}(G_{sr}(X_s))).$$

Here, H_s denotes entropy under the simulator-induced distribution. The conditional entropy term is not directly available, but it can be bounded using a variational approximation $q(\Theta | G_{rs}(G_{sr}(X_s)))$. By the non-negativity of the conditional Kullback–Leibler (KL) divergence, [33, 34]:

$$I_s(\Theta; G_{rs}(G_{sr}(X_s))) \geq H_s(\Theta) + \mathbb{E}_{(\Theta, X_s) \sim p_s} [\log q(\Theta | G_{rs}(G_{sr}(X_s)))]. \quad (2)$$

The bound is exact when $q(\Theta | G_{rs}(G_{sr}(X_s)))$ equals the true conditional posterior. The expectation term increases when the variational posterior assigns higher density to the original simulator parameter after transport. This leads to the information-preservation loss, defined as the negative of the expectation term in Eq. (2):

$$\mathcal{L}_{\text{info}}(q) := \mathbb{E}_{(\Theta, X_s) \sim p_s} \left[-\log q(\Theta | G_{rs}(G_{sr}(X_s))) \right]. \quad (3)$$

Since $H_s(\Theta)$ is fixed, minimizing $\mathcal{L}_{\text{info}}$ maximizes the lower bound above. During transport training, this objective updates G_{rs} and G_{sr} so that the transported simulator observation remains informative about the original parameter.

If the learned transports match the observation distributions across domains and maintain the statistical dependence encouraged by $\mathcal{L}_{\text{info}}$, the simulator-to-real component satisfies the population-level condition

$$(\Theta, X_r) \stackrel{d}{=} (\Theta, G_{sr}(X_s)), \quad (\Theta, X_s) \sim p_s(\theta, x_s). \quad (4)$$

That is, $G_{sr}(X_s)$ is matched to X_r jointly with the parameter. Under this condition, the learned real-to-simulator transport G_{rs} can be applied to real-world observations x_r at test time while preserving parameter-relevant information. This corresponds to the inference rule in Eq. (1). Appendix A formalizes this connection by showing that, under Eq. (4), the real-world test-time risk equals the simulator-labeled transported risk used by L_{info} .

2.3 Training objective

SPIN jointly trains the transport networks, discriminators, and posterior estimator. The full training procedure is provided in Algorithm 1 in Appendix C.

Generator loss. The generator loss combines adversarial translation, cycle-consistency, identity regularization [30], and information preservation:

$$\mathcal{L}_G = \lambda_{\text{adv}} \mathcal{L}_{\text{adv}}^G + \lambda_{\text{cyc}} \mathcal{L}_{\text{cyc}} + \lambda_{\text{id}} \mathcal{L}_{\text{id}} + \lambda_{\text{info}} \mathbb{E}_{(\theta, x_s) \sim p_s(\theta, x_s)} [-\log q_{\text{sg}(\psi, \omega)}(\theta | x_{sr_s})].$$

Here, $\text{sg}(\cdot)$ denotes the stop-gradient operator, and $q_{\text{sg}(\psi, \omega)}$ indicates that the summary network and posterior estimator are held fixed during the generator update. Thus, the information-preservation term updates only the transport networks G_{rs} and G_{sr} .

Discriminator loss. The discriminators use hinge adversarial losses with spectral normalization [35]:

$$\mathcal{L}_D = \mathcal{L}_{\text{adv}}^D.$$

Posterior loss. The posterior estimator is trained on both original simulated observations and transported observations with simulator labels:

$$\mathcal{L}_{\text{NPE}} = \mathcal{L}_s(q_\psi) + \lambda_{\text{info}} \mathbb{E}_{(\theta, x_s) \sim p_s(\theta, x_s)} [-\log q_\psi(\theta | \text{sg}(x_{sr_s}))].$$

Here, $\text{sg}(x_{sr_s})$ keeps the transported observations fixed. This update extends posterior training to transported simulator-domain inputs, while preventing the posterior loss from changing the transport itself.

Unless otherwise stated, we set $\lambda_{\text{info}} = 1$. This assigns the transported observation with a simulator label the same negative conditional log-likelihood weight as the original simulator observation, without selecting the constraint strength using real-world labels. Figure 1 summarizes the training and inference procedure.

3 Experiments

We evaluate SPIN in the unlabeled, unpaired real-world adaptation regime. Real-world parameter labels, when available in controlled benchmarks, are used only for evaluation.

3.1 Benchmarks

Additional dataset and simulation details are provided in Appendix B.

SIR. SIR [36] is a weakly misspecified synthetic benchmark used in recent robust SBI evaluations and based on a discrete-time stochastic susceptible–infected–recovered model [14, 18, 21]. The parameter is

$$\theta = (\beta, \gamma),$$

where β denotes the infection rate and γ denotes the recovery rate. Misspecification arises from delayed weekend reporting, where a fraction of Saturday and Sunday infections is shifted to Monday.

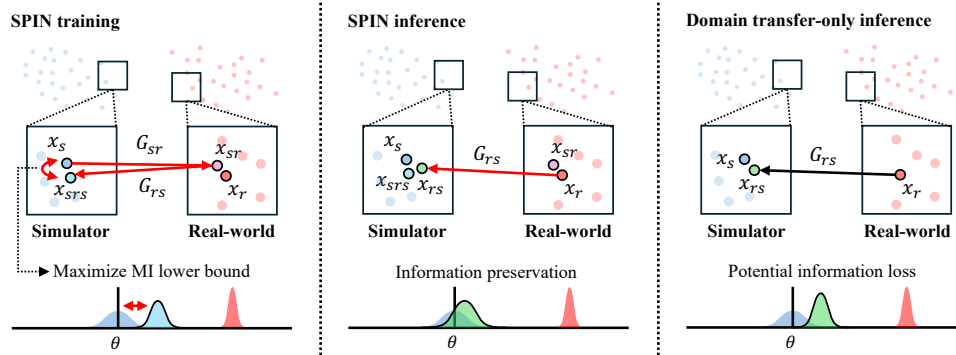


Figure 1: **Overview of SPIN.** During training, a labeled simulator observation (θ, x_s) is translated toward the real-world domain as x_{sr} and returned to the simulator domain as x_{srs} . Since x_{srs} retains the simulator-origin label, SPIN uses θ to maximize the MI lower bound in Eq. (2), encouraging parameter-relevant information to be preserved after transport. At test time, an unlabeled real-world observation x_r is mapped to the simulator domain as $x_{rs} = G_{rs}(x_r)$, and inference is performed as $q_\psi(\theta | x_{rs})$. The right panel illustrates that domain transfer alone can match domains while losing information needed for posterior inference.

Pendulum. Pendulum is a controlled synthetic benchmark used in prior misspecified SBI studies [14, 18]. The synthetic real-world domain introduces damping while preserving the same parameter value

$$\theta = (\omega_0, \phi),$$

where ω_0 denotes the natural angular frequency and ϕ denotes the initial phase. The damping coefficient α is sampled from a continuous range so that the benchmark reflects a continuum of misspecification.

Wind Tunnel. Wind Tunnel evaluates a controlled physical simulator–reality gap in a wind-chamber system. This benchmark uses the controlled wind-tunnel setup from Causal Chambers [37], which has been used for misspecified SBI evaluation [14, 18]. Following the benchmark setup, the inference target is

$$\theta = H,$$

where H denotes the hatch position controlling the wind-tunnel opening. The simulator captures the main physical mechanism, whereas misspecification arises because the mechanistic model only approximates the real chamber response to fan loads and hatch position.

Light Tunnel. Light Tunnel also evaluates a controlled physical simulator–reality gap, here in an optical imaging system. This benchmark uses the controlled light-tunnel setup from Causal Chambers [37], which has also been used in prior misspecified SBI benchmarks [14, 18]. The inference target is

$$\theta = (R, G, B, \alpha),$$

where (R, G, B) denote the light-source color intensities and α denotes the polarizer-induced dimming factor. The simulator captures the dominant optical mechanism, whereas misspecification arises from simplified modeling of the real light-tunnel response.

3.2 Baselines

We compare SPIN to standard NPE [3, 4] and two unlabeled domain-alignment methods, NPE-MMD [21] and NPE-DANN [21]. NPE uses only labeled simulations, whereas NPE-MMD and NPE-DANN also use unlabeled real-world observations for adaptation. We use NPE-MMD rather than NPE-RS [12] because the original NPE-RS formulation is not fully amortized. Across methods, the same summary network and posterior flow are used within each task.

RoPE [14] and FRISBI [18] are not included as baselines because they use a small real-world calibration set with known parameters. NPE+SC [13] is also not included as a baseline because it relies on Bayesian self-consistency [19, 20] with likelihood evaluations or an auxiliary likelihood

estimator. Related methods are summarized in Appendix D.1. Implementation details, architectures, and optimization settings are provided in Appendix C.

3.3 Evaluation protocol

Real-world parameter labels are reserved exclusively for evaluation and are never used during adaptation. Unless otherwise stated, quantitative results are reported as mean \pm standard deviation over five independent training runs with different random seeds. Posterior means and sample-based posterior-discrepancy metrics are computed using 1000 posterior samples per observation.

Main metrics. We evaluate real-world posterior quality using root mean squared error (RMSE), log posterior probability (LPP), and ACAUC, defined as the signed area between the empirical coverage curve and the nominal coverage diagonal [14, 18]. RMSE of posterior means measures point-estimation accuracy, with lower values indicating that posterior mass is centered closer to the ground-truth parameter. LPP evaluates the posterior density assigned to the ground-truth parameter [38]. It is the evaluation metric closest in form to the information-preservation objective, because both LPP and $\mathcal{L}_{\text{info}}$ depend on the posterior density assigned to the corresponding parameter value. From the variational information-maximization perspective, this posterior-density term acts as the tractable energy term in a lower bound on parameter-relevant mutual information, with the entropy term fixed within each task [33, 34]. Thus, higher LPP can be interpreted as stronger posterior-based information transmission from the posterior input to the parameter, up to the variational approximation described in Appendix A.2. ACAUC is used as a scalar posterior diagnostic based on expected-coverage analysis [39]. We interpret ACAUC together with RMSE and LPP, because global diagnostics provide only a partial check of posterior quality. The corresponding diagnostic curves are reported in Appendix D.5. Appendix D.3 further evaluates the simulator-originated transported observations x_{srs} , where $\mathcal{L}_{\text{info}}$ is directly applied, using RMSE, LPP, and ACAUC. To assess sensitivity to misspecification strength, we vary the Pendulum damping coefficient and evaluate RMSE, LPP, and ACAUC across damping levels.

We report symmetric KL divergence (sKL) [40], Wasserstein distance [41], and posterior MMD [22] together in Appendix D.2 as secondary posterior-discrepancy diagnostics, computed between simulator-side posteriors and real-world posteriors for matched simulated and real-world observations.

To evaluate the contribution of parameter-relevant information preservation, we include a transport-only variant, SPIN (w/o $\mathcal{L}_{\text{info}}$), which keeps the same bidirectional transport architecture but removes the information-preservation term. Comparing this variant with SPIN tests whether simulator-labeled conditional density supervision on transported observations improves real-world posterior quality.

Ablation study. We vary N_r to assess the dependence of SPIN on the amount of unlabeled real-world data used for adaptation. This analysis evaluates sensitivity to the size of the real-world adaptation set, including settings with limited real-world observations. We additionally vary λ_{info} in Appendix D.6 (Figure 9) to examine the sensitivity of the method to the strength of information-preservation supervision.

4 Results and Discussion

4.1 Main results

Table 1 summarizes the quantitative results across the four benchmarks. Overall, SPIN showed a more stable performance profile across RMSE, LPP, and ACAUC than the marginal domain-alignment baselines. Appendix D.7 provides qualitative transport examples as visual diagnostics of the learned observation-space transport.

NPE-MMD and NPE-DANN improved over standard NPE in some settings, but their gains were not uniform across tasks and metrics. In comparison, SPIN improved the main posterior-quality metrics more consistently on Pendulum, Wind Tunnel, and Light Tunnel. This indicates that real-world posterior inference benefits not only from reducing domain discrepancy, but also from domain transport that preserves information relevant to the parameter.

This effect is most directly reflected in LPP. The LPP gains on Pendulum, Wind Tunnel, and Light Tunnel therefore support the intended information-preserving role of real-to-simulator transport.

Table 1: Main benchmark results on the four tasks. Results are reported as mean \pm standard deviation over runs. Lower is better for RMSE, higher is better for LPP, and ACAUC is best when closer to zero.

Task	Metric	NPE	NPE-MMD	NPE-DANN	SPIN (w/o $\mathcal{L}_{\text{info}}$)	SPIN
SIR	RMSE	0.059 \pm 0.005	0.058 \pm 0.001	0.059 \pm 0.002	0.060 \pm 0.006	0.059 \pm 0.003
	LPP	4.002 \pm 0.226	4.043 \pm 0.463	4.235 \pm 0.281	3.350 \pm 1.797	3.775 \pm 0.757
	ACAUC	-0.032 \pm 0.014	-0.033 \pm 0.022	-0.048 \pm 0.010	-0.011 \pm 0.029	-0.025 \pm 0.016
Pendulum	RMSE	0.774 \pm 0.217	0.514 \pm 0.140	0.572 \pm 0.097	0.344 \pm 0.069	0.287 \pm 0.062
	LPP	-49.89 \pm 19.17	-89.53 \pm 68.95	-57.02 \pm 72.97	-8.341 \pm 6.824	-4.327 \pm 3.914
	ACAUC	0.265 \pm 0.078	0.220 \pm 0.058	0.185 \pm 0.053	0.077 \pm 0.063	0.062 \pm 0.063
Wind Tunnel	RMSE	7.768 \pm 0.893	4.108 \pm 0.928	4.345 \pm 0.654	4.128 \pm 0.438	4.098 \pm 0.433
	LPP	-43.02 \pm 16.61	-26.33 \pm 10.62	-27.43 \pm 14.42	-26.96 \pm 8.059	-10.04 \pm 1.412
	ACAUC	0.417 \pm 0.013	0.304 \pm 0.052	0.317 \pm 0.039	0.344 \pm 0.025	0.280 \pm 0.020
Light Tunnel	RMSE	66.16 \pm 11.38	57.51 \pm 2.727	47.56 \pm 7.008	40.41 \pm 3.226	35.33 \pm 0.871
	LPP ($\times 10^3$)	-3.626 \pm 2.522	-2.394 \pm 0.221	-1.404 \pm 0.649	-0.536 \pm 0.087	-0.124 \pm 0.013
	ACAUC	0.326 \pm 0.027	0.246 \pm 0.019	0.211 \pm 0.052	0.187 \pm 0.017	0.163 \pm 0.017

The accompanying RMSE and ACAUC gains indicate that the LPP improvement is not only a density-level effect. Posterior means also move closer to the reference parameters, while the coverage diagnostic shows improved uncertainty behavior. Appendix D.3 reports the corresponding check on x_{sts} , where the effect of $\mathcal{L}_{\text{info}}$ should be most directly observed. The higher LPP of SPIN on this path confirms that $\mathcal{L}_{\text{info}}$ behaves as intended on the labeled simulator-originated observations.

SIR showed smaller differences among methods. This is consistent with a boundary case where standard NPE already provides a strong reference point, leaving less room for adaptation to improve posterior inference. Similar behavior has been reported in FRISBI, where standard NPE can be sufficient under minimal misspecification [18]. In such settings, additional alignment or transport objectives may yield smaller or less consistent gains because adaptation introduces optimization and regularization trade-offs [21].

On Pendulum, Wind Tunnel, and Light Tunnel, adding $\mathcal{L}_{\text{info}}$ improved the main inference metrics compared with SPIN (w/o $\mathcal{L}_{\text{info}}$). This pattern indicates that the improvement is not only due to bidirectional transport, but also to the information-preservation constraint imposed by $\mathcal{L}_{\text{info}}$, which encourages transported observations to remain informative about the corresponding simulator parameter.

The posterior-discrepancy diagnostics in Appendix D.2 provide secondary support for this interpretation. SPIN reduced sKL on the benchmarks with larger simulator–reality gaps, indicating reduced posterior-level disagreement between matched simulator and real-world observations. Wasserstein distance and posterior MMD showed broadly consistent but task-dependent patterns, suggesting that this effect is not limited to a single discrepancy measure.

4.2 Sensitivity to misspecification strength

The Pendulum benchmark allows the strength of model misspecification to be controlled through the damping coefficient. Figure 2 shows qualitative posterior comparisons on matched Pendulum examples under increasing misspecification. As damping increased, direct inference on the real-world observation produced posteriors with less mass near the reference parameter, whereas SPIN placed posterior mass closer to the reference parameter after real-to-simulator transport.

Figure 3 summarizes the corresponding quantitative trend. Under weak shift, all adaptation methods were relatively close, while SPIN remained competitive. As damping increased, the gains of SPIN became clearer, particularly in LPP while maintaining favorable RMSE and ACAUC. Together, the posterior examples and quantitative metrics indicate that the benefit of SPIN becomes clearer as misspecification increases. This within-task trend is consistent with the cross-benchmark pattern in Table 1, where SPIN showed clearer improvements on Pendulum and on the controlled physical simulator–reality gaps in Wind Tunnel and Light Tunnel than on weakly misspecified SIR.

The comparison with SPIN (w/o $\mathcal{L}_{\text{info}}$) shows how the contribution of simulator-labeled information-preservation supervision changes with misspecification strength. The performance gap between the two variants became larger under stronger damping. As the simulator–reality gap increases, marginal

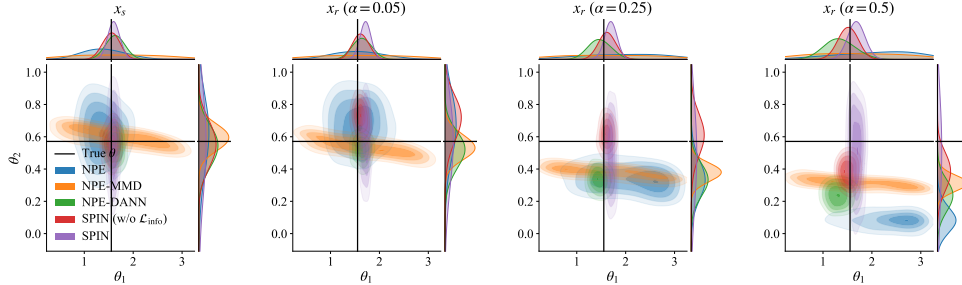


Figure 2: **Posterior comparison across methods on matched Pendulum samples under increasing misspecification.** Each column shows a matched simulator/real-world example sharing the same parameter, with the real-world observation generated under a different damping strength α . In the stronger damping settings, SPIN shows posterior mass closer to the reference parameter. These examples provide qualitative posterior comparisons under increasing misspecification and complement the RMSE, LPP, and ACAUC results in Table 1.

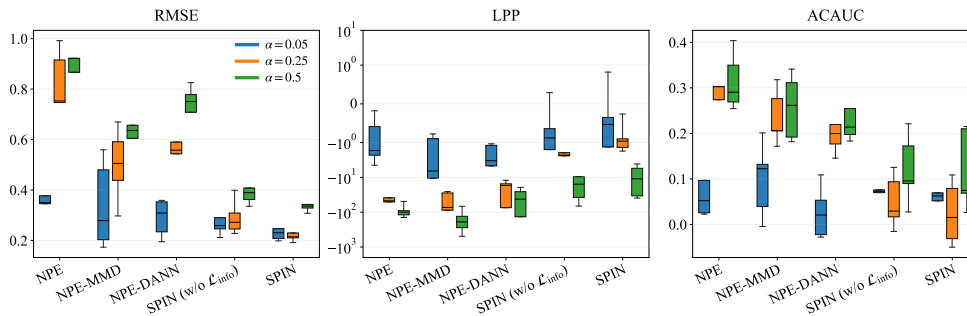


Figure 3: **Sensitivity to misspecification strength on Pendulum.** Box plots summarize performance over five independent runs at three damping levels $\alpha \in \{0.05, 0.25, 0.5\}$. Under weak shift, methods are relatively close, while SPIN shows clearer gains as damping increases. SPIN (w/o $\mathcal{L}_{\text{info}}$) removes simulator-labeled information-preservation supervision, highlighting the contribution of $\mathcal{L}_{\text{info}}$ under stronger misspecification.

alignment can reduce domain discrepancy, but it does not ensure preservation of the relation between the physical parameter and the posterior input [24, 25, 26]. This trend is therefore consistent with the intended role of $\mathcal{L}_{\text{info}}$, which becomes most useful when misspecification is large enough.

4.3 Training dynamics of the information-preservation objective

Figure 4 provides an additional analysis of the training dynamics of $\mathcal{L}_{\text{info}}$ in Eq. (3). We compare SPIN with its transport-only variant, SPIN (w/o $\mathcal{L}_{\text{info}}$), where the same quantity is monitored but not used as a transport constraint.

The difference between the two variants was smallest on weakly misspecified SIR and larger on Pendulum and on the controlled physical simulator–reality gaps in Wind Tunnel and Light Tunnel. This trend is consistent with the main results. The effect of information-preservation supervision becomes more visible as the simulator–reality gap increases. The training dynamics therefore provide supporting evidence for the improvements observed in Table 1 and Figure 3. The simulator-side NPE loss \mathcal{L}_s is reported in Appendix D.4.

4.4 Sensitivity to the amount of unlabeled real-world data

We evaluated how SPIN changes with N_r , the number of unlabeled real-world observations used during adaptation. Figure 5 shows that the effect of the real-world data budget depends on the task and metric. SIR and Wind Tunnel showed relatively small variation across budgets. Pendulum showed clearer changes in LPP and ACAUC, whereas Light Tunnel was more sensitive to very small real-world budgets, especially in RMSE and LPP.

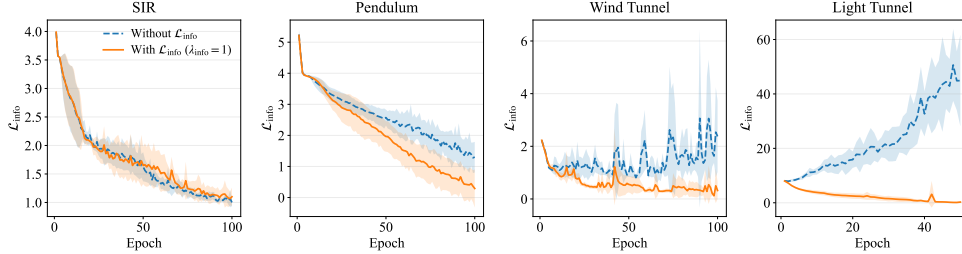


Figure 4: **Effect of information-preservation supervision during training.** We plot the mean over five runs together with run-to-run variability for $\mathcal{L}_{\text{info}}$ in Eq. (3), comparing the transport-only variant ($\lambda_{\text{info}} = 0$) with the full method ($\lambda_{\text{info}} = 1$). The difference is smallest on SIR and becomes larger on Pendulum, Wind Tunnel, and Light Tunnel.

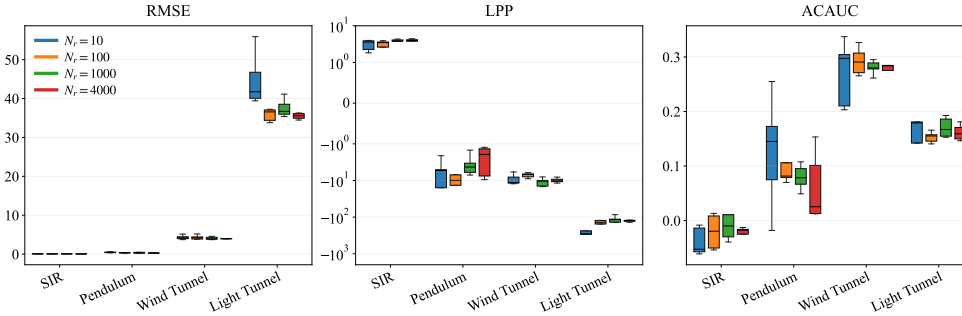


Figure 5: **Performance across unlabeled real-world data budgets.** We vary N_r , the number of unlabeled real-world observations used during adaptation, while keeping N_s fixed, and report performance across tasks over five independent runs. The effect of the real-world data budget depends on the task and metric.

This pattern is consistent with the role of unlabeled real-world observations in SPIN. The real-world pool provides samples from the target observation distribution used to train simulator-to-real transport. In particular, G_{sr} is trained so that simulator-originated observations are translated toward the empirical real-world distribution, which in turn defines the real-like inputs on which the return transport G_{rs} is constrained. When N_r is very small, this empirical target distribution can be estimated only coarsely, which can make transport learning less stable, especially under larger simulator–reality gaps. Together, these results indicate that sufficient coverage of the real-world observation distribution is important for stable transport learning, but that posterior quality remains task- and metric-dependent rather than being determined by N_r alone.

4.5 Limitations

Several limitations should be considered. First, if the learned transport poorly approximates the parameter-preserving joint-transport condition in Eq. (4), real-world inference after transport can be degraded. This issue is related to how well the unlabeled real-world pool represents the target observation distribution for simulator-to-real transport. With small N_r , this empirical distribution can be estimated only coarsely, especially under larger simulator–reality gaps, which can make transport learning less stable. Second, $\lambda_{\text{info}} = 1$ provides a label-free equal-weight default between original and transported simulator observations, but the optimal weight may be task-dependent. Sensitivity to this choice is reported in Appendix D.6. Finally, SPIN adds training-time cost through transport and discriminator updates, while preserving amortized inference at test time. Computational costs are summarized in Table 4.

5 Conclusion

We introduced SPIN for misspecified SBI with unlabeled, unpaired real-world observations. SPIN learns information-preserving bidirectional domain transport and performs posterior inference after

mapping real-world observations to the simulator domain. Instead of relying only on marginal domain alignment, SPIN encourages domain transfer that preserves MI between the parameter of interest and the transported observations. Across synthetic and controlled physical benchmarks, SPIN improved point accuracy, posterior density at the reference parameter used for evaluation, and expected-coverage diagnostics, with the clearest gains appearing under stronger misspecification. These results suggest that domain transport for misspecified SBI may benefit from explicitly preserving parameter-relevant information, in addition to reducing marginal discrepancy between simulated and real-world data.

References

- [1] Kyle Cranmer, Johann Brehmer, and Gilles Louppe. The frontier of simulation-based inference. *Proceedings of the National Academy of Sciences*, 117(48):30055–30062, 2020. doi: 10.1073/pnas.1912789117. URL <https://doi.org/10.1073/pnas.1912789117>.
- [2] Michael Deistler, Jan Boelts, Peter Steinbach, Guy Moss, Thomas Moreau, Manuel Gloeckler, Pedro L. C. Rodrigues, Julia Linhart, Janne K. Lappalainen, Benjamin Kurt Miller, Pedro J. Gonçalves, Jan-Matthis Lueckmann, Cornelius Schröder, and Jakob H. Macke. Simulation-based inference: A practical guide, 2025. URL <https://arxiv.org/abs/2508.12939>.
- [3] George Papamakarios and Iain Murray. Fast ϵ -free inference of simulation models with Bayesian conditional density estimation. In *Advances in Neural Information Processing Systems*, volume 29, pages 1028–1036, 2016. URL <https://proceedings.neurips.cc/paper/2016/hash/6aca97005c68f1206823815f66102863-Abstract.html>.
- [4] David S. Greenberg, Marcel Nonnenmacher, and Jakob H. Macke. Automatic posterior transformation for likelihood-free inference. In *Proceedings of the 36th International Conference on Machine Learning*, volume 97 of *Proceedings of Machine Learning Research*, pages 2404–2414, 2019. URL <https://proceedings.mlr.press/v97/greenberg19a.html>.
- [5] George E. P. Box. Science and statistics. *Journal of the American Statistical Association*, 71(356):791–799, 1976. doi: 10.1080/01621459.1976.10480949. URL <https://doi.org/10.1080/01621459.1976.10480949>.
- [6] David T. Frazier, Christian P. Robert, and Judith Rousseau. Model misspecification in approximate bayesian computation: Consequences and diagnostics. *Journal of the Royal Statistical Society: Series B (Statistical Methodology)*, 82(2):421–444, 2020. doi: 10.1111/rssb.12356. URL <https://doi.org/10.1111/rssb.12356>.
- [7] Patrick Cannon, Daniel Ward, and Sebastian M. Schmon. Investigating the impact of model misspecification in neural simulation-based inference, 2022. URL <https://arxiv.org/abs/2209.01845>.
- [8] B. J. K. Kleijn and A. W. van der Vaart. The bernstein-von mises theorem under misspecification. *Electronic Journal of Statistics*, 6:354–381, 2012. doi: 10.1214/12-EJS675. URL <https://doi.org/10.1214/12-EJS675>.
- [9] Andrew Gelman, Xiao-Li Meng, and Hal Stern. Posterior predictive assessment of model fitness via realized discrepancies. *Statistica Sinica*, 6(4):733–807, 1996. URL <https://www3.stat.sinica.edu.tw/statistica/j6n4/j6n41/j6n41.htm>.
- [10] Daniel Ward, Patrick Cannon, Mark Beaumont, Matteo Fasiolo, and Sebastian M. Schmon. Robust neural posterior estimation and statistical model criticism. In *Advances in Neural Information Processing Systems*, volume 35, pages 33845–33859, 2022. URL <https://neurips.cc/virtual/2022/poster/52936>.
- [11] Marvin Schmitt, Paul-Christian Bürkner, Ullrich Köthe, and Stefan T Radev. Detecting model misspecification in amortized bayesian inference with neural networks. In *Dagm german conference on pattern recognition*, pages 541–557. Springer, 2023. URL <https://arxiv.org/pdf/2112.08866>.

- [12] Daolang Huang, Ayush Bharti, Amauri H. Souza, Luigi Acerbi, and Samuel Kaski. Learning robust statistics for simulation-based inference under model misspecification. In *Advances in Neural Information Processing Systems*, volume 36, 2023. URL https://proceedings.neurips.cc/paper_files/paper/2023/hash/16c5b4102a6b6eb061e502ce6736ad8a-Abstract-Conference.html.
- [13] Marvin Schmitt, Desi Ivanova, Daniel Habermann, Paul-Christian Bürkner, Ullrich Köthe, and Stefan T. Radev. Robust amortized bayesian inference with self-consistency losses on unlabeled data. In *International Conference on Learning Representations*, 2026. URL <https://openreview.net/forum?id=E1dANKwo4I>.
- [14] Antoine Wehenkel, Juan L. Gamella, Ozan Sener, Jens Behrmann, Guillermo Sapiro, Jörn-Henrik Jacobsen, and Marco Cuturi. Addressing misspecification in simulation-based inference through data-driven calibration. In *Proceedings of the 42nd International Conference on Machine Learning*, volume 267 of *Proceedings of Machine Learning Research*, 2025. URL <https://openreview.net/forum?id=y3d4Bs2r7r>.
- [15] Nicolas Courty, Rémi Flamary, Devis Tuia, and Alain Rakotomamonjy. Optimal transport for domain adaptation. *IEEE Transactions on Pattern Analysis and Machine Intelligence*, 39(9):1853–1865, 2017. doi: 10.1109/TPAMI.2016.2615921. URL <https://doi.org/10.1109/TPAMI.2016.2615921>.
- [16] Cédric Villani. *Optimal Transport: Old and New*, volume 338 of *Grundlehren der mathematischen Wissenschaften*. Springer, Berlin, Heidelberg, 2009. doi: 10.1007/978-3-540-71050-9. URL <https://doi.org/10.1007/978-3-540-71050-9>.
- [17] Gabriel Peyré and Marco Cuturi. *Computational optimal transport: With applications to data science*. Now Foundations and Trends, 2019. URL <https://arxiv.org/abs/1803.00567>.
- [18] Ortal Senouf, Antoine Wehenkel, Cédric Vincent-Cuaz, Emmanuel Abbé, and Pascal Frossard. Inductive domain transfer in misspecified simulation-based inference. In *Advances in Neural Information Processing Systems*, 2025. URL <https://openreview.net/forum?id=PhnquAa8eV>.
- [19] Marvin Schmitt, Desi Ivanova, Daniel Habermann, Paul-Christian Bürkner, Ullrich Köthe, and Stefan T. Radev. Leveraging self-consistency for data-efficient amortized bayesian inference. In *Proceedings of the 41st International Conference on Machine Learning*, volume 235 of *Proceedings of Machine Learning Research*, pages 43723–43741. PMLR, 2024. URL <https://proceedings.mlr.press/v235/schmitt24a.html>.
- [20] Desi R. Ivanova, Marvin Schmitt, and Stefan T. Radev. Data-efficient variational mutual information estimation via bayesian self-consistency. In *NeurIPS 2024 Workshop on Bayesian Decision-making and Uncertainty*, 2024. URL <https://openreview.net/forum?id=QfiyE1a01f>.
- [21] Lasse Elsemüller, Valentin Pratz, Mischa von Krause, Andreas Voss, Paul-Christian Bürkner, and Stefan T. Radev. Does unsupervised domain adaptation improve the robustness of amortized bayesian inference? a systematic evaluation. *Transactions on Machine Learning Research*, 2025. URL <https://openreview.net/forum?id=ewgLuvnEw6>.
- [22] Arthur Gretton, Karsten M. Borgwardt, Malte J. Rasch, Bernhard Schölkopf, and Alexander Smola. A kernel two-sample test. *Journal of Machine Learning Research*, 13(25):723–773, 2012. URL <https://jmlr.org/papers/v13/gretton12a.html>.
- [23] Yaroslav Ganin, Evgeniya Ustinova, Hana Ajakan, Pascal Germain, Hugo Larochelle, François Laviolette, Mario Marchand, and Victor Lempitsky. Domain-adversarial training of neural networks. *Journal of Machine Learning Research*, 17(59):1–35, 2016. URL <https://jmlr.org/papers/v17/15-239.html>.
- [24] Fredrik D. Johansson, David Sontag, and Rajesh Ranganath. Support and invertibility in domain-invariant representations. In *Proceedings of the 22nd International Conference on Artificial Intelligence and Statistics*, volume 89 of *Proceedings of Machine Learning Research*, pages 527–536, 2019. URL <https://proceedings.mlr.press/v89/johansson19a.html>.

- [25] Han Zhao, Remi Tachet des Combes, Kun Zhang, and Geoffrey J. Gordon. On learning invariant representations for domain adaptation. In *Proceedings of the 36th International Conference on Machine Learning*, volume 97 of *Proceedings of Machine Learning Research*, pages 7523–7532, 2019. URL <https://proceedings.mlr.press/v97/zhao19a.html>.
- [26] Petar Stojanov, Zijian Li, Mingming Gong, Ruichu Cai, Jaime Carbonell, and Kun Zhang. Domain adaptation with invariant representation learning: What transformations to learn? In M. Ranzato, A. Beygelzimer, Y. Dauphin, P.S. Liang, and J. Wortman Vaughan, editors, *Advances in Neural Information Processing Systems*, volume 34, pages 24791–24803. Curran Associates, Inc., 2021. URL https://proceedings.neurips.cc/paper_files/paper/2021/file/cfc5d9422f0c8f8ad796711102dbe32b-Paper.pdf.
- [27] Judy Hoffman, Eric Tzeng, Taesung Park, Jun-Yan Zhu, Phillip Isola, Kate Saenko, Alexei Efros, and Trevor Darrell. CyCADA: Cycle-consistent adversarial domain adaptation. In Jennifer Dy and Andreas Krause, editors, *Proceedings of the 35th International Conference on Machine Learning*, volume 80 of *Proceedings of Machine Learning Research*, pages 1989–1998. PMLR, 10–15 Jul 2018. URL <https://proceedings.mlr.press/v80/hoffman18a.html>.
- [28] Stefan T. Radev, Ulf K. Mertens, Andreas Voss, Lynton Ardizzone, and Ullrich Köthe. BayesFlow: Learning complex stochastic models with invertible neural networks. *IEEE Transactions on Neural Networks and Learning Systems*, 33(4):1452–1466, 2022. doi: 10.1109/TNNLS.2020.3042395. URL <https://doi.org/10.1109/TNNLS.2020.3042395>.
- [29] Yanzhi Chen, Dinghuai Zhang, Michael U. Gutmann, Aaron Courville, and Zhanxing Zhu. Neural approximate sufficient statistics for implicit models. In *International Conference on Learning Representations*, 2021. URL <https://openreview.net/forum?id=SRDuJssQud>.
- [30] Jun-Yan Zhu, Taesung Park, Phillip Isola, and Alexei A. Efros. Unpaired image-to-image translation using cycle-consistent adversarial networks. In *Proceedings of the IEEE International Conference on Computer Vision*, pages 2223–2232, 2017. doi: 10.1109/ICCV.2017.244. URL <https://doi.org/10.1109/ICCV.2017.244>.
- [31] Claude E. Shannon. A mathematical theory of communication. *The Bell System Technical Journal*, 27(3–4):379–423, 623–656, 1948. doi: 10.1002/j.1538-7305.1948.tb01338.x. URL <https://doi.org/10.1002/j.1538-7305.1948.tb01338.x>.
- [32] Thomas M. Cover and Joy A. Thomas. *Elements of Information Theory*. Wiley-Interscience, Hoboken, NJ, 2 edition, 2006. doi: 10.1002/047174882X. URL <https://doi.org/10.1002/047174882X>.
- [33] David Barber and Felix V. Agakov. The IM algorithm: A variational approach to information maximization. In *Advances in Neural Information Processing Systems*, volume 16, 2003. URL https://aivalley.com/Papers/MI_NIPS_final.pdf.
- [34] Ben Poole, Sherjil Ozair, Aaron van den Oord, Alexander A. Alemi, and George Tucker. On variational bounds of mutual information. In *Proceedings of the 36th International Conference on Machine Learning*, volume 97 of *Proceedings of Machine Learning Research*, pages 5171–5180, 2019. URL <https://proceedings.mlr.press/v97/poole19a.html>.
- [35] Takeru Miyato, Toshiki Kataoka, Masanori Koyama, and Yuichi Yoshida. Spectral normalization for generative adversarial networks. In *International Conference on Learning Representations*, 2018. URL <https://openreview.net/forum?id=B1QRgziT->.
- [36] William Ogilvy Kermack and Anderson G. McKendrick. A contribution to the mathematical theory of epidemics. *Proceedings of the Royal Society of London. Series A, Containing Papers of a Mathematical and Physical Character*, 115(772):700–721, 1927. doi: 10.1098/rspa.1927.0118. URL <https://doi.org/10.1098/rspa.1927.0118>.
- [37] Juan L. Gamella, Jonas Peters, and Peter Bühlmann. Causal chambers as a real-world physical testbed for AI methodology. *Nature Machine Intelligence*, 7:107–118, 2025. doi: 10.1038/s42256-024-00964-x. URL <https://doi.org/10.1038/s42256-024-00964-x>.

- [38] Jan-Matthis Lueckmann, Jan Boelts, David S. Greenberg, Pedro J. Gonçalves, and Jakob H. Macke. Benchmarking simulation-based inference. In *Proceedings of the 24th International Conference on Artificial Intelligence and Statistics*, volume 130 of *Proceedings of Machine Learning Research*, pages 343–351, 2021. URL <https://proceedings.mlr.press/v130/lueckmann21a.html>.
- [39] Joeri Hermans, Arnaud Delaunoy, François Rozet, Antoine Wehenkel, Volodimir Begy, and Gilles Louppe. A crisis in simulation-based inference? beware, your posterior approximations can be unfaithful. *Transactions on Machine Learning Research*, 2022. URL <https://openreview.net/forum?id=LHAbHkt6Aq>.
- [40] Solomon Kullback and Richard A. Leibler. On information and sufficiency. *The Annals of Mathematical Statistics*, 22(1):79–86, 1951. doi: 10.1214/aoms/1177729694. URL <https://doi.org/10.1214/aoms/1177729694>.
- [41] Aaditya Ramdas, Nicolás García Trillos, and Marco Cuturi. On wasserstein two-sample testing and related families of nonparametric tests. *Entropy*, 19(2):47, 2017. doi: 10.3390/e19020047. URL <https://doi.org/10.3390/e19020047>.
- [42] Edward Collett. *Field Guide to Polarization*. SPIE Press, Bellingham, WA, 2005. doi: 10.1117/3.626141. URL <https://doi.org/10.1117/3.626141>.
- [43] Ilya Tolstikhin, Olivier Bousquet, Sylvain Gelly, and Bernhard Schölkopf. Wasserstein auto-encoders. In *International Conference on Learning Representations*, 2018. URL <https://openreview.net/forum?id=HkL7n1-0b>.
- [44] George Papamakarios, Theo Pavlakou, and Iain Murray. Masked autoregressive flow for density estimation. In *Advances in Neural Information Processing Systems*, volume 30, pages 2335–2344, 2017. URL <https://proceedings.neurips.cc/paper/2017/hash/6c1da886822c67822bcf3679d04369fa-Abstract.html>.
- [45] François Rozet, Felix Divo, and Simon Schnake. *probabilists/zuko: Zuko 1.1.0*, January 2024. URL <https://doi.org/10.5281/zenodo.10571785>.
- [46] Ilya Loshchilov and Frank Hutter. Decoupled weight decay regularization. In *International Conference on Learning Representations*, 2019. URL <https://openreview.net/forum?id=Bkg6RiCqY7>.
- [47] Diederik P. Kingma and Jimmy Ba. Adam: A method for stochastic optimization. In *International Conference on Learning Representations*, 2015. URL <https://arxiv.org/abs/1412.6980>.
- [48] Samantha R. Cook, Andrew Gelman, and Donald B. Rubin. Validation of software for bayesian models using posterior quantiles. *Journal of Computational and Graphical Statistics*, 15(3):675–692, 2006. doi: 10.1198/106186006X136976. URL <https://doi.org/10.1198/106186006X136976>.
- [49] Sean Talts, Michael Betancourt, Daniel Simpson, Aki Vehtari, and Andrew Gelman. Validating bayesian inference algorithms with simulation-based calibration, 2018. URL <https://arxiv.org/abs/1804.06788>.

A Mathematical details for parameter-relevant information preservation

This appendix collects the population identities used to interpret the information-preservation objective. The identities clarify when simulator-label supervision on transported observations corresponds to the conditional log-risk of the real-world test-time rule, and why the same log-score is aligned with the information-preservation interpretation used in the main text.

A.1 Population identity for the test-time rule

Let $(\Theta, X_s) \sim P_s$ denote the simulator joint distribution on $\Theta \times \mathcal{X}_s$, and let $(\Theta, X_r) \sim P_r$ denote the real-world joint distribution on $\Theta \times \mathcal{X}_r$. During training, real-world samples are observed only through X_r ; the variable Θ under P_r is used only to define population risks and evaluation quantities.

For any posterior estimator q , define the real-world test-time conditional log-risk

$$\mathcal{R}_r(q, G_{rs}) = \mathbb{E}_{(\Theta, X_r) \sim P_r} [-\log q(\Theta \mid G_{rs}(X_r))],$$

and the simulator-labeled transported risk

$$\mathcal{R}_{\text{tr}}(q, G_{sr}, G_{rs}) = \mathbb{E}_{(\Theta, X_s) \sim P_s} [-\log q(\Theta \mid G_{rs}(G_{sr}(X_s)))].$$

The information-preservation objective in Eq. (3) is

$$\mathcal{L}_{\text{info}}(q) = \mathcal{R}_{\text{tr}}(q, G_{sr}, G_{rs}).$$

The population condition connecting the simulator-originated training route and the real-world test-time route is the parameter-preserving joint-transport condition

$$(\Theta, X_r) \stackrel{d}{=} (\Theta, G_{sr}(X_s)), \quad (\Theta, X_s) \sim P_s. \quad (5)$$

This condition is stronger than matching only the observation marginal. Marginal alignment can make $G_{sr}(X_s)$ and X_r similar as observations, but it does not by itself specify whether the transported observation preserves its relation to Θ [24, 25]. The same distinction applies after a summary network: marginally matching $h_\omega(G_{sr}(X_s))$ and $h_\omega(X_r)$ does not imply joint matching with the parameter [24, 25, 26].

Proposition 1 (Risk identity under parameter-preserving joint transport). *If Eq. (5) holds, then for any posterior estimator q and any real-to-simulator transport G_{rs} ,*

$$\mathcal{R}_r(q, G_{rs}) = \mathcal{R}_{\text{tr}}(q, G_{sr}, G_{rs}) = \mathcal{L}_{\text{info}}(q).$$

Proof. By Eq. (5), the random pairs (Θ, X_r) and $(\Theta, G_{sr}(X_s))$ have the same distribution. Therefore, for any measurable function f with finite expectation,

$$\mathbb{E}_{(\Theta, X_r) \sim P_r} [f(\Theta, X_r)] = \mathbb{E}_{(\Theta, X_s) \sim P_s} [f(\Theta, G_{sr}(X_s))].$$

Choosing

$$f(\theta, x) = -\log q(\theta \mid G_{rs}(x))$$

gives

$$\mathbb{E}_{(\Theta, X_r) \sim P_r} [-\log q(\Theta \mid G_{rs}(X_r))] = \mathbb{E}_{(\Theta, X_s) \sim P_s} [-\log q(\Theta \mid G_{rs}(G_{sr}(X_s)))].$$

The left-hand side is $\mathcal{R}_r(q, G_{rs})$, and the right-hand side is $\mathcal{R}_{\text{tr}}(q, G_{sr}, G_{rs}) = \mathcal{L}_{\text{info}}(q)$. \square

Proposition 1 is a population identity under the stated joint-transport condition. It does not assert that a learned finite-data transport necessarily satisfies this condition. In the main experiments, this condition is encouraged by adversarial translation, cycle consistency, identity regularization, and the simulator-label information-preservation objective, and the resulting inference quality is evaluated empirically.

A.2 Log-score objective and information preservation

The information-preservation objective is a simulator-label log-score on the transported simulator observation. Applying the standard log-score decomposition to the posterior input $G_{rs}(G_{sr}(X_s))$ gives

$$\begin{aligned}\mathcal{L}_{\text{info}}(q) &= \mathbb{E}_{(\Theta, X_s) \sim P_s} [-\log q(\Theta \mid G_{rs}(G_{sr}(X_s)))] \\ &= H_s(\Theta \mid G_{rs}(G_{sr}(X_s))) + \mathbb{E}[\text{KL}(p_s(\Theta \mid G_{rs}(G_{sr}(X_s))) \parallel q(\Theta \mid G_{rs}(G_{sr}(X_s))))].\end{aligned}$$

Here, the conditional distribution is induced by $(\Theta, X_s) \sim P_s$. Since $H_s(\Theta)$ is fixed by the simulator prior,

$$I_s(\Theta; G_{rs}(G_{sr}(X_s))) = H_s(\Theta) - H_s(\Theta \mid G_{rs}(G_{sr}(X_s))).$$

Thus, minimizing the optimal simulator-label log-score on $G_{rs}(G_{sr}(X_s))$ reduces the conditional entropy of the parameter given the transported simulator observation. With finite model capacity, $\mathcal{L}_{\text{info}}$ serves as a supervised log-score surrogate for preserving parameter-relevant information after transport.

The same log-score interpretation applies to the real-world test-time input. For SPIN, real-world inference is performed from $G_{rs}(X_r)$, so the corresponding population log-risk is

$$\begin{aligned}\mathcal{R}_r(q, G_{rs}) &= \mathbb{E}_{(\Theta, X_r) \sim P_r} [-\log q(\Theta \mid G_{rs}(X_r))] \\ &= H_r(\Theta \mid G_{rs}(X_r)) + \mathbb{E}[\text{KL}(p_r(\Theta \mid G_{rs}(X_r)) \parallel q(\Theta \mid G_{rs}(X_r)))].\end{aligned}$$

Therefore,

$$H_r(\Theta) + \mathbb{E}_{(\Theta, X_r) \sim P_r} [\log q(\Theta \mid G_{rs}(X_r))] \leq I_r(\Theta; G_{rs}(X_r)),$$

with gap

$$\mathbb{E}[\text{KL}(p_r(\Theta \mid G_{rs}(X_r)) \parallel q(\Theta \mid G_{rs}(X_r)))].$$

This is the population quantity approximated by LPP [38] on the real-world test set. Within a task, $H_r(\Theta)$ is fixed, so comparing this expected log posterior density across methods is equivalent to comparing the corresponding posterior-based information lower bound up to an additive constant. We use this only as an interpretation of the posterior log-score, not as an independent mutual-information estimator.

B Dataset and benchmark details

Across all tasks in the main experiments, we use the same split sizes for simulator and real-world observations. Specifically, $N_s = 4000$ simulator observations are used for training, with 500 additional simulator observations used for validation and 500 for testing. Similarly, $N_r = 4000$ real-world observations are used for training, with 500 additional real-world observations used for validation and 500 for testing.

SIR. SIR is a weakly misspecified synthetic benchmark based on a discrete-time stochastic susceptible–infected–recovered model [36]. We fix the population size and initial infected count to

$$N = 1000, \quad I_0 = 10,$$

and sample parameters from

$$\beta \sim \mathcal{U}[0.05, 0.5], \quad \gamma \sim \mathcal{U}[0.05, 0.5],$$

subject to the constraint $\beta > \gamma$. The simulator records daily new infections for $T = 365$ days. Transitions are sampled with binomial draws. The real-world domain is generated from the same parameter values, but the daily counts are modified by a simple reporting-delay mechanism: on Saturdays and Sundays, 5% of the reported infections are delayed, and the delayed mass is added back on Monday.

Pendulum. Pendulum is a synthetic benchmark in which the simulator is a frictionless pendulum integrated with an Euler solver, while the real-world domain introduces damping. For data generation, we first sample

$$\omega_0 \sim \mathcal{U}\left[\frac{\pi}{10}, \pi\right], \quad \phi_0 \sim \mathcal{U}\left[-\frac{\pi}{2}, \frac{\pi}{2}\right],$$

and an initial angular velocity

$$\dot{\theta}_0 \sim \mathcal{U}[-1, 1].$$

The simulator uses zero damping, whereas the synthetic real-world data use

$$\alpha \sim \mathcal{U}[0.05, 0.5].$$

The Euler integrator is run for $T = 200$ output steps over $T_{\max} = 10$ seconds with inner step size $\Delta t_{\text{inner}} = 0.01$, which yields 5 inner Euler updates per reported observation step. Gaussian observation noise with standard deviation 0.05 is added in both domains.

Wind Tunnel. Wind Tunnel uses the `wt_intake_impulse_v1` dataset from Causal Chambers [37], with experiment `load_out_0.5_osr_downwind_4`. Each real observation is constructed as one impulse response extracted from the downwind barometer trace. The real impulse rows are shuffled once with a fixed permutation and then split into train/validation/test subsets.

For simulation, we use the mechanistic A2C3 wind-tunnel model. We sample the hatch position uniformly:

$$H \sim \mathcal{U}[0, 45].$$

The misspecification reflects the gap between the mechanistic A2C3 model and the measured chamber response to fan loads and hatch position.

Light Tunnel. Light Tunnel uses the `1t_camera_v1` dataset from Causal Chambers [37], with experiment `uniform_ap_1.8_iso_500.0_ss_0.005`. For each real image, the dataset provides light-source RGB values (R, G, B) and polarizer angles $(\text{pol}_1, \text{pol}_2)$. We convert the polarizer angles to

$$\alpha = \cos^2((\text{pol}_1 - \text{pol}_2)\pi/180)$$

using Malus’ law [42]. Thus,

$$R, G, B \in [0, 255], \quad \alpha \in [0, 1].$$

For the simulated domain, we use the F3 light-tunnel model and sample

$$R, G, B \sim \mathcal{U}[0, 255], \quad \alpha \sim \mathcal{U}[0, 1].$$

The sampled dimming variable is converted to a polarizer-angle pair $(0, \Delta)$ with

$$\Delta = \arccos(\sqrt{\alpha}) \cdot \frac{180}{\pi}.$$

The simulator then renders the image using the stored camera sensitivity curves, white-balance coefficients, exposure value, and tunnel geometry constants. The misspecification reflects the gap between this simplified optical model and the measured real light-tunnel response.

C Implementation details and computational cost

Baseline training. NPE [3, 4] trains the summary network and conditional flow jointly by minimizing the negative conditional log-likelihood on simulated pairs (θ, x_s) . NPE-MMD [21] uses the same architecture and optimizer as NPE and adds an inverse-multiquadratic MMD (IMQ-MMD) [22] penalty between simulated and real summary features. We use the standard multi-scale IMQ kernel [43] with scales $\{0.1, 0.2, 0.5, 1, 2, 5, 10\}$. NPE-DANN [21] also uses the same summary network and posterior flow, and adds a domain classifier with 3 hidden layers of width 256. Domain confusion is applied through a gradient reversal layer with the standard schedule [23]

$$\lambda_{\text{grl}}(p) = \frac{2}{1 + \exp(-10p)} - 1,$$

where p is the normalized training progress. The domain classifier is trained jointly with the summary network and posterior flow using binary cross-entropy.

Parameterization and posterior family. For all tasks, the parameters are bounded. We therefore map parameters θ to an unconstrained latent variable u with a componentwise logit transform and train the posterior model in u -space. The posterior estimator is a conditional masked autoregressive flow (MAF) implemented with zuko [44, 45]. For all tasks, the conditioner depth is fixed to 3. At evaluation time, posterior samples are transformed back to the parameter space through the inverse sigmoid map. Table 2 summarizes the main training hyperparameters.

Optimization. For NPE, NPE-MMD, and NPE-DANN, we optimize the summary network and posterior flow with AdamW [46]. For NPE-DANN, the domain classifier is optimized jointly with the same AdamW optimizer. For SPIN, we use three optimizers: (i) Adam [47] for the generators, (ii) Adam for the discriminators, and (iii) AdamW for the summary network and posterior flow. For the generator and discriminator optimizers, we use $\beta_1 = 0.5$ and $\beta_2 = 0.999$. The generator/discriminator learning rate is fixed to 0.0002 in all tasks, while the posterior optimizer uses the task-specific learning rate from Table 2.

Table 2: **Task-specific training hyperparameters used in the main experiments.**

	SIR	Pendulum	Wind Tunnel	Light Tunnel
Epochs	100	100	100	100
Batch size B	100	100	100	10
Learning rate	5×10^{-4}	1×10^{-4}	5×10^{-4}	5×10^{-4}
Weight decay	1×10^{-4}	1×10^{-4}	1×10^{-4}	1×10^{-4}
Embedding dim	6	10	10	20

Summary networks. The posterior flow is conditioned on a task-specific summary network [2, 28, 29]. For Pendulum and Wind Tunnel, we use 1D convolutional summary networks following encoder architectures used in prior misspecified SBI work [14, 18]. For SIR, we use a compact 1D convolutional summary network, and for Light Tunnel we use a 2D convolutional summary network operating directly on RGB images. Table 3 lists the task-specific summary networks used in all methods for each task.

Table 3: **Task-specific summary networks.**

Task	Architecture
SIR	Summary network: 1D CNN with conv stack $1 \rightarrow 16 \rightarrow 64 \rightarrow 128 \rightarrow 128 \rightarrow 128$, kernel sizes $(5, 5, 3, 3, 3)$, strides $(1, 2, 1, 2, 1)$, dilation 2 in the last three convolutions, average pooling after the 2nd and 4th convolutions, and adaptive average pooling to length 8. The head is an MLP $\text{flat} \rightarrow 256 \rightarrow 128 \rightarrow 6$ with ReLU activations.
Pendulum	Summary network: 1D CNN with conv stack $1 \rightarrow 16 \rightarrow 64 \rightarrow 128 \rightarrow 128 \rightarrow 128 \rightarrow 128$, kernel size 3, dilation 2, strided layers at the 2nd, 4th, and 6th convolutions, and average pooling after the 2nd, 4th, and 6th convolutions. The convolutional trunk is followed by an MLP $\text{flat} \rightarrow 512 \rightarrow 128 \rightarrow 32 \rightarrow 10$ with ReLU activations.
Wind Tunnel	Summary network: 1D CNN with conv stack $1 \rightarrow 8 \rightarrow 32 \rightarrow 64 \rightarrow 64 \rightarrow 64 \rightarrow 64$, kernel size 3, dilation 2, strided layers at the 2nd, 4th, and 6th convolutions, average pooling after the 2nd, 4th, and 6th convolutions, and an MLP $\text{flat} \rightarrow 256 \rightarrow 64 \rightarrow 16 \rightarrow 10$ with ReLU activations.
Light Tunnel	Summary network: 2D CNN with conv stack $3 \rightarrow 48 \rightarrow 96 \rightarrow 128$ using kernels $(5, 3, 3)$ with stride 2 at every convolution, followed by adaptive average pooling to 4×4 , then an MLP $\text{flat} \rightarrow 128 \rightarrow 20$ with ReLU activations.

SPIN generators and discriminators. For SPIN, we use bidirectional observation-space translators G_{sr} and G_{rs} together with one discriminator per domain [30]. For the 1D tasks, both translators use the same architecture: a stem convolution $1 \rightarrow 32$ with kernel size 7, two downsampling convolutions $32 \rightarrow 64 \rightarrow 128$ with stride 2, a bottleneck composed of 4 residual blocks with dilation schedule (1, 2, 4, 8), and two upsampling stages with linear interpolation and 3×1 convolutions $128 \rightarrow 64 \rightarrow 32$, followed by a 7×1 output convolution. The final prediction is combined with the input through a learned residual skip:

$$y = \sigma(a)x + (1 - \sigma(a))\hat{y}.$$

For the 2D image task, both translators use a 2D analogue of the same design with channels $3 \rightarrow 32 \rightarrow 64 \rightarrow 128$, bilinear upsampling, and 4 residual bottleneck blocks.

For the 1D tasks, the discriminator trunk is $1 \rightarrow 32 \rightarrow 64 \rightarrow 128 \rightarrow 128$ with LeakyReLU activations and a fused patch/global head. For the 2D task, the discriminator trunk is $3 \rightarrow 32 \rightarrow 64 \rightarrow 128 \rightarrow 128$ with the same patch/global fusion design. Spectral normalization [35] is enabled in all discriminators.

Training algorithm. Algorithm 1 summarizes the SPIN training loop, including the generator, discriminator, and posterior updates performed for each mini-batch.

Algorithm 1 Training procedure for SPIN

Require: simulated training pairs $\{(\theta_i, x_i^s)\}$, unlabeled real training pool $\{x_j^r\}$, summary network h_ω , posterior flow q_ψ , translators G_{sr}, G_{rs} , discriminators D_R, D_S

- 1: Initialize $h_\omega, q_\psi, G_{sr}, G_{rs}, D_R, D_S$
- 2: **for** epoch = $1, \dots, E$ **do**
- 3: **for** mini-batch **do**
- 4: Sample simulated batch (θ, x_s) and unlabeled real batch x_r
- 5: **Generator step:**
- 6: $x_{sr} \leftarrow G_{sr}(x_s), x_{rs} \leftarrow G_{rs}(x_r)$
- 7: $x_{srs} \leftarrow G_{rs}(G_{sr}(x_s)), x_{rst} \leftarrow G_{sr}(G_{rs}(x_r))$
- 8: Compute adversarial, cycle-consistency, and identity losses
- 9: Compute information-preservation loss $-\log q_\psi(\theta | h_\omega(x_{srs}))$
- 10: Form $\mathcal{L}_G = \lambda_{adv} \mathcal{L}_{adv}^G + \lambda_{cyc} \mathcal{L}_{cyc} + \lambda_{id} \mathcal{L}_{id} + \lambda_{info} [-\log q_{sg(\psi, \omega)}(\theta | x_{srs})]$
- 11: Update G_{sr}, G_{rs} by descending $\nabla_{G_{sr}, G_{rs}} \mathcal{L}_G$
- 12: **Discriminator step:**
- 13: Form $\mathcal{L}_D = \mathcal{L}_{adv}^D$ with hinge losses on real and translated samples
- 14: Update D_R, D_S by descending $\nabla_{D_R, D_S} \mathcal{L}_D$
- 15: **Posterior step:**
- 16: Recompute x_{srs} without gradient through the translators
- 17: Compute

$$\mathcal{L}_{NPE} = -\log q_\psi(\theta | h_\omega(x_s)) + \lambda_{info} [-\log q_\psi(\theta | h_\omega(x_{srs}))]$$
- 18: Update h_ω, q_ψ
- 19: **end for**
- 20: Evaluate simulator-side validation NPE loss on $(\theta_{val}, x_{val}^s)$
- 21: **end for**
- 22: Use $q_\psi(\theta | x_{rs})$ for test-time inference

Compute environment. All experiments were run on a single NVIDIA RTX A6000 GPU unless stated otherwise. SPIN is computationally heavier than NPE, NPE-MMD, and NPE-DANN because each mini-batch includes generator, discriminator, and posterior updates. This cost affects training only; test-time inference remains amortized and uses a single real-to-simulator transport followed by posterior evaluation.

Computational cost. We compare the computational cost of all methods in Table 4. The table reports trainable parameters, average training time per iteration, and amortized inference time per observation. Training time includes all updates used by each method, and inference time is measured for posterior evaluation with 1000 samples per observation.

Table 4: **Model size and computational cost.** We report trainable parameters, average training time per iteration, and amortized inference time per observation. Training time includes all updates used by each method. Inference time is measured for posterior evaluation with 1000 samples per observation.

Task	Method	Trainable parameters	Training time / iteration	Inference time / obs.
SIR	NPE	467,324	6.49 ± 0.04 ms	3.79 ± 0.39 ms
	NPE-MMD	467,324	11.67 ± 0.05 ms	3.76 ± 0.30 ms
	NPE-DANN	600,957	8.88 ± 0.05 ms	3.58 ± 0.01 ms
	SPIN	1,606,672	100.91 ± 0.09 ms	5.32 ± 0.09 ms
Pendulum	NPE	1,387,744	14.93 ± 0.35 ms	5.59 ± 0.05 ms
	NPE-MMD	1,387,744	24.86 ± 0.46 ms	5.60 ± 0.04 ms
	NPE-DANN	1,522,401	21.30 ± 0.31 ms	5.65 ± 0.03 ms
	SPIN	2,527,092	323.30 ± 81.20 ms	6.97 ± 1.00 ms
Wind Tunnel	NPE	112,250	7.25 ± 0.06 ms	2.27 ± 0.19 ms
	NPE-MMD	112,250	12.69 ± 0.03 ms	2.13 ± 0.02 ms
	NPE-DANN	246,907	10.10 ± 0.04 ms	2.14 ± 0.03 ms
	SPIN	1,251,598	96.31 ± 0.56 ms	3.88 ± 0.47 ms
Light Tunnel	NPE	1,454,308	6.49 ± 0.16 ms	8.54 ± 0.48 ms
	NPE-MMD	1,454,308	13.40 ± 0.41 ms	8.69 ± 0.66 ms
	NPE-DANN	1,591,525	9.66 ± 0.86 ms	7.96 ± 0.02 ms
	SPIN	4,981,842	99.66 ± 0.34 ms	9.27 ± 0.04 ms

D Additional experimental results and analyses

D.1 Comparison of related methods

Table 5 summarizes the related methods discussed in the main text.

Table 5: **Comparison of related misspecified SBI methods.** The table summarizes whether each method uses real-world data, whether it requires a calibration set with known parameters, whether inference is fully amortized, and the main mechanism used to handle model misspecification. Here, a calibration set denotes real-world observations with known parameters.

Method	Real-world data	Calibration set	Amortized	Approach
NPE [3, 4]	None	No	Yes	Simulator-only inference
RoPE [14]	Yes	Yes	Not fully	Optimal transport
FRISBI [18]	Yes	Yes	Yes	Optimal transport
NPE+SC [13]	Yes	No	Yes	Bayesian self-consistency
NPE-RS [12]	Yes	No	Not fully	MMD-based domain alignment
NPE-MMD [21]	Yes	No	Yes	MMD-based domain alignment
NPE-DANN [21]	Yes	No	Yes	Adversarial domain alignment
SPIN	Yes	No	Yes	Information-preserving domain transfer

D.2 Posterior-discrepancy diagnostics

Table 6 reports secondary posterior-discrepancy diagnostics corresponding to the analysis described in the main text.

Table 6: **Posterior-discrepancy diagnostics.** We report symmetric Kullback–Leibler divergence (sKL) [40], Wasserstein distance [41], and posterior MMD [22] as secondary diagnostics computed between simulator-side posteriors and method-specific real-world posteriors for matched simulated and real-world observations. On the more clearly misspecified Pendulum, Wind Tunnel, and Light Tunnel benchmarks, SPIN reduces sKL and often improves the auxiliary discrepancy measures, with task-dependent differences across Wasserstein distance and posterior MMD.

Task	Metric	NPE	NPE-MMD	NPE-DANN	SPIN (w/o $\mathcal{L}_{\text{info}}$)	SPIN
SIR	sKL	2.82 ± 0.13	2.58 ± 0.30	2.70 ± 0.29	3.65 ± 0.88	3.19 ± 0.64
	Wasserstein	0.0046 ± 0.0003	0.0041 ± 0.0007	0.0040 ± 0.0005	0.0401 ± 0.0029	0.0046 ± 0.0002
	MMD	0.0012 ± 0.0000	0.0012 ± 0.0000	0.0012 ± 0.0000	0.2011 ± 0.0271	0.0012 ± 0.0000
Pendulum	sKL	26.51 ± 5.45	25.59 ± 7.81	19.57 ± 7.01	10.13 ± 2.70	9.76 ± 4.86
	Wasserstein	0.559 ± 0.158	0.284 ± 0.075	0.398 ± 0.062	0.229 ± 0.027	0.224 ± 0.027
	MMD	0.7310 ± 0.0710	0.5350 ± 0.3590	0.5430 ± 0.1560	0.3540 ± 0.1020	0.4030 ± 0.1410
Wind Tunnel	sKL	28.51 ± 5.35	14.80 ± 5.13	16.85 ± 4.00	19.31 ± 4.39	10.86 ± 2.75
	Wasserstein	5.667 ± 0.862	2.968 ± 0.576	3.269 ± 0.377	3.129 ± 0.289	3.277 ± 0.508
	MMD	1.2430 ± 0.1470	0.7810 ± 0.1870	0.8540 ± 0.1410	0.9390 ± 0.1330	0.6640 ± 0.1090
Light Tunnel	sKL	37.31 ± 6.33	28.82 ± 0.42	26.72 ± 3.86	24.62 ± 2.11	21.38 ± 1.01
	Wasserstein	51.158 ± 12.456	41.089 ± 3.134	29.013 ± 8.909	25.717 ± 4.879	17.868 ± 0.823
	MMD	1.0210 ± 0.0960	0.8020 ± 0.0560	0.5840 ± 0.2520	0.5070 ± 0.1250	0.3190 ± 0.0250

D.3 Evaluation on transported simulator observations

Figure 6 evaluates x_{srs} using RMSE, LPP, and ACAUC. Since x_{srs} is generated from labeled simulator samples, this analysis checks whether $\mathcal{L}_{\text{info}}$ increases the posterior density assigned to the original simulator parameter on the transported observations it directly supervises.

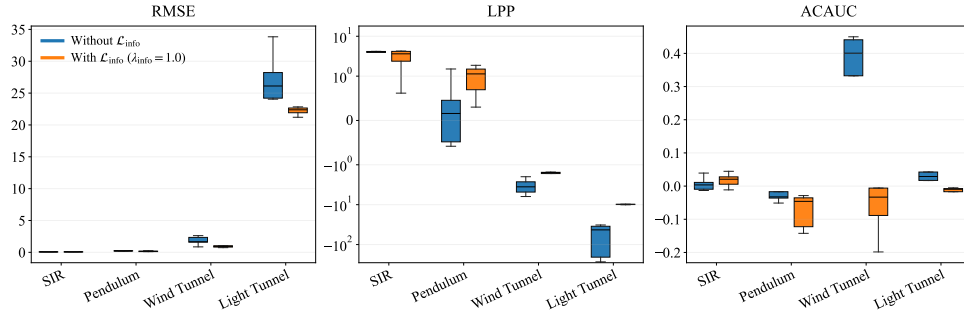


Figure 6: **Evaluation on transported simulator observations.** We evaluate x_{srs} using RMSE, LPP, and ACAUC over five independent runs. Since x_{srs} is generated from labeled simulator samples, the original simulator label remains available for evaluation. The comparison between SPIN and SPIN (w/o $\mathcal{L}_{\text{info}}$) therefore serves as a diagnostic for the simulator-originated training path, showing what is gained by adding $\mathcal{L}_{\text{info}}$ to the shared bidirectional transport architecture.

D.4 Optimization dynamics

Figure 7 reports the simulator-side NPE risk \mathcal{L}_s for $\lambda_{\text{info}} = 0$ and $\lambda_{\text{info}} = 1$.

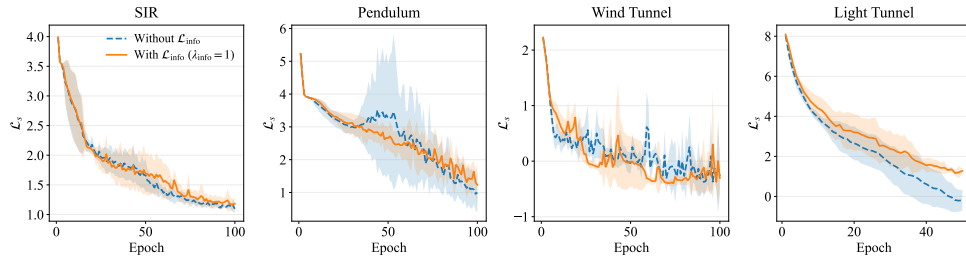


Figure 7: **Simulator-side risk dynamics.** We plot the median over five runs together with run-to-run variability for the simulator-side NPE risk \mathcal{L}_s , comparing $\lambda_{\text{info}} = 0$ and $\lambda_{\text{info}} = 1$. This analysis shows that adding information-preservation supervision preserves the simulator-side posterior training anchor.

D.5 Calibration analysis

Figure 8 reports the calibration curves corresponding to the ACAUC values used in the main results [14, 18, 48, 49].

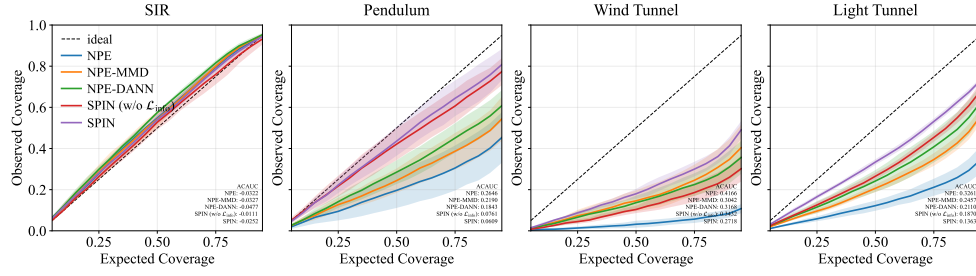


Figure 8: **Calibration analysis.** Marginal calibration curves and ACAUC values for the four tasks. Curves closer to the diagonal indicate better empirical coverage. SPIN improves or maintains calibration on the more strongly misspecified benchmarks, while differences are smaller on weakly misspecified SIR where the simulator-trained posterior is already competitive.

D.6 Sensitivity to information-preservation strength

Figure 9 varies the strength of information-preservation supervision while keeping the rest of the training setup fixed.

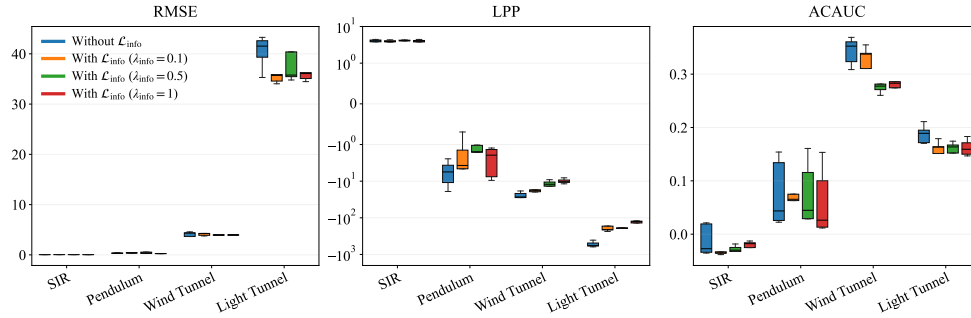


Figure 9: **Sensitivity analysis of λ_{info} .** We report the effect of varying λ_{info} across tasks. Unlike Figure 4, which isolates the presence or absence of the information-preservation term, this figure shows that the most effective information-preservation strength can be task-dependent. In particular, weakly misspecified settings such as SIR may require little or only moderate information-preservation pressure, whereas more clearly misspecified tasks benefit more consistently from stronger information-preservation constraints.

D.7 Qualitative transport examples

Figure 10 visualizes the learned observation-space transport and is included only as qualitative support.

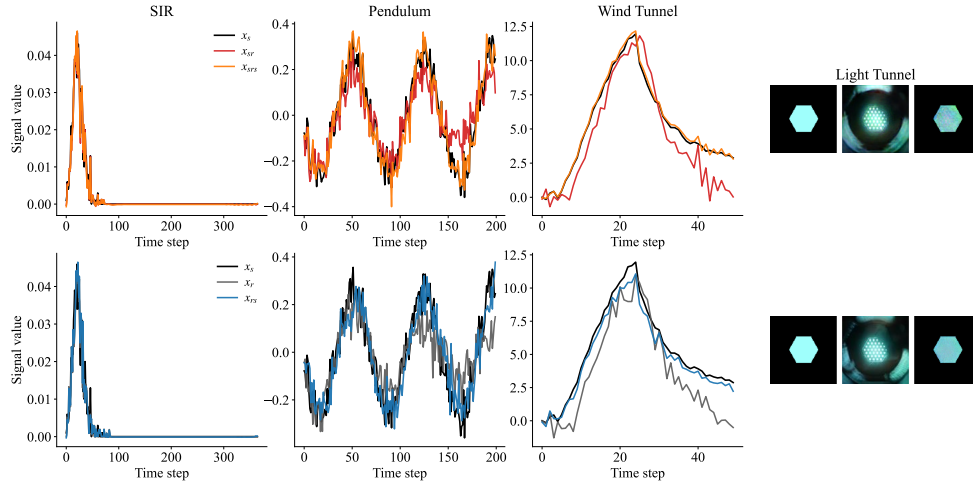


Figure 10: **Additional qualitative transport examples.** Representative examples of simulated observations x_s , real-world observations x_r , simulator-to-real transported observations x_{sr} , and real-to-simulator transported observations x_{rs} . These panels illustrate the learned observation-space transport, particularly on the more structured visual domain shifts. Visual alignment alone does not certify the joint parameter–observation alignment required by SPIN, but these examples provide qualitative support for the learned observation-space transport.

NeurIPS Paper Checklist

1. Claims

Question: Do the main claims made in the abstract and introduction accurately reflect the paper’s contributions and scope?

Answer: [Yes]

Justification: The main claims are stated in the abstract and Introduction.

Guidelines:

- The answer [N/A] means that the abstract and introduction do not include the claims made in the paper.
- The abstract and/or introduction should clearly state the claims made, including the contributions made in the paper and important assumptions and limitations. A [No] or [N/A] answer to this question will not be perceived well by the reviewers.
- The claims made should match theoretical and experimental results, and reflect how much the results can be expected to generalize to other settings.
- It is fine to include aspirational goals as motivation as long as it is clear that these goals are not attained by the paper.

2. Limitations

Question: Does the paper discuss the limitations of the work performed by the authors?

Answer: [Yes]

Justification: Limitations are discussed in the Limitations section.

Guidelines:

- The answer [N/A] means that the paper has no limitation while the answer [No] means that the paper has limitations, but those are not discussed in the paper.
- The authors are encouraged to create a separate “Limitations” section in their paper.
- The paper should point out any strong assumptions and how robust the results are to violations of these assumptions (e.g., independence assumptions, noiseless settings, model well-specification, asymptotic approximations only holding locally). The authors should reflect on how these assumptions might be violated in practice and what the implications would be.
- The authors should reflect on the scope of the claims made, e.g., if the approach was only tested on a few datasets or with a few runs. In general, empirical results often depend on implicit assumptions, which should be articulated.
- The authors should reflect on the factors that influence the performance of the approach. For example, a facial recognition algorithm may perform poorly when image resolution is low or images are taken in low lighting. Or a speech-to-text system might not be used reliably to provide closed captions for online lectures because it fails to handle technical jargon.
- The authors should discuss the computational efficiency of the proposed algorithms and how they scale with dataset size.
- If applicable, the authors should discuss possible limitations of their approach to address problems of privacy and fairness.
- While the authors might fear that complete honesty about limitations might be used by reviewers as grounds for rejection, a worse outcome might be that reviewers discover limitations that aren’t acknowledged in the paper. The authors should use their best judgment and recognize that individual actions in favor of transparency play an important role in developing norms that preserve the integrity of the community. Reviewers will be specifically instructed to not penalize honesty concerning limitations.

3. Theory assumptions and proofs

Question: For each theoretical result, does the paper provide the full set of assumptions and a complete (and correct) proof?

Answer: [Yes]

Justification: The assumptions and proof are provided in Appendix A.

Guidelines:

- The answer [N/A] means that the paper does not include theoretical results.
- All the theorems, formulas, and proofs in the paper should be numbered and cross-referenced.
- All assumptions should be clearly stated or referenced in the statement of any theorems.
- The proofs can either appear in the main paper or the supplemental material, but if they appear in the supplemental material, the authors are encouraged to provide a short proof sketch to provide intuition.
- Inversely, any informal proof provided in the core of the paper should be complemented by formal proofs provided in appendix or supplemental material.
- Theorems and Lemmas that the proof relies upon should be properly referenced.

4. Experimental result reproducibility

Question: Does the paper fully disclose all the information needed to reproduce the main experimental results of the paper to the extent that it affects the main claims and/or conclusions of the paper (regardless of whether the code and data are provided or not)?

Answer: [Yes]

Justification: Reproducibility details are provided in the Experiments section and Appendix C.

Guidelines:

- The answer [N/A] means that the paper does not include experiments.
- If the paper includes experiments, a [No] answer to this question will not be perceived well by the reviewers: Making the paper reproducible is important, regardless of whether the code and data are provided or not.
- If the contribution is a dataset and/or model, the authors should describe the steps taken to make their results reproducible or verifiable.
- Depending on the contribution, reproducibility can be accomplished in various ways. For example, if the contribution is a novel architecture, describing the architecture fully might suffice, or if the contribution is a specific model and empirical evaluation, it may be necessary to either make it possible for others to replicate the model with the same dataset, or provide access to the model. In general, releasing code and data is often one good way to accomplish this, but reproducibility can also be provided via detailed instructions for how to replicate the results, access to a hosted model (e.g., in the case of a large language model), releasing of a model checkpoint, or other means that are appropriate to the research performed.
- While NeurIPS does not require releasing code, the conference does require all submissions to provide some reasonable avenue for reproducibility, which may depend on the nature of the contribution. For example
 - (a) If the contribution is primarily a new algorithm, the paper should make it clear how to reproduce that algorithm.
 - (b) If the contribution is primarily a new model architecture, the paper should describe the architecture clearly and fully.
 - (c) If the contribution is a new model (e.g., a large language model), then there should either be a way to access this model for reproducing the results or a way to reproduce the model (e.g., with an open-source dataset or instructions for how to construct the dataset).
 - (d) We recognize that reproducibility may be tricky in some cases, in which case authors are welcome to describe the particular way they provide for reproducibility. In the case of closed-source models, it may be that access to the model is limited in some way (e.g., to registered users), but it should be possible for other researchers to have some path to reproducing or verifying the results.

5. Open access to data and code

Question: Does the paper provide open access to the data and code, with sufficient instructions to faithfully reproduce the main experimental results, as described in supplemental material?

Answer: [Yes]

Justification: Code and experiment scripts are available for all reported experiments, and data generation or processing instructions are available for the Pendulum and Causal Chambers benchmarks. The code will be made publicly available upon acceptance.

Guidelines:

- The answer [N/A] means that paper does not include experiments requiring code.
- Please see the NeurIPS code and data submission guidelines (<https://neurips.cc/public/guides/CodeSubmissionPolicy>) for more details.
- While we encourage the release of code and data, we understand that this might not be possible, so [No] is an acceptable answer. Papers cannot be rejected simply for not including code, unless this is central to the contribution (e.g., for a new open-source benchmark).
- The instructions should contain the exact command and environment needed to run to reproduce the results. See the NeurIPS code and data submission guidelines (<https://neurips.cc/public/guides/CodeSubmissionPolicy>) for more details.
- The authors should provide instructions on data access and preparation, including how to access the raw data, preprocessed data, intermediate data, and generated data, etc.
- The authors should provide scripts to reproduce all experimental results for the new proposed method and baselines. If only a subset of experiments are reproducible, they should state which ones are omitted from the script and why.
- At submission time, to preserve anonymity, the authors should release anonymized versions (if applicable).
- Providing as much information as possible in supplemental material (appended to the paper) is recommended, but including URLs to data and code is permitted.

6. Experimental setting/details

Question: Does the paper specify all the training and test details (e.g., data splits, hyperparameters, how they were chosen, type of optimizer) necessary to understand the results?

Answer: [Yes]

Justification: Experimental settings are described in the Experiments section and Appendix C.

Guidelines:

- The answer [N/A] means that the paper does not include experiments.
- The experimental setting should be presented in the core of the paper to a level of detail that is necessary to appreciate the results and make sense of them.
- The full details can be provided either with the code, in appendix, or as supplemental material.

7. Experiment statistical significance

Question: Does the paper report error bars suitably and correctly defined or other appropriate information about the statistical significance of the experiments?

Answer: [Yes]

Justification: Error bars and variability across runs are described in the Evaluation protocol and reported in the results.

Guidelines:

- The answer [N/A] means that the paper does not include experiments.
- The authors should answer [Yes] if the results are accompanied by error bars, confidence intervals, or statistical significance tests, at least for the experiments that support the main claims of the paper.
- The factors of variability that the error bars are capturing should be clearly stated (for example, train/test split, initialization, random drawing of some parameter, or overall run with given experimental conditions).
- The method for calculating the error bars should be explained (closed form formula, call to a library function, bootstrap, etc.)

- The assumptions made should be given (e.g., Normally distributed errors).
- It should be clear whether the error bar is the standard deviation or the standard error of the mean.
- It is OK to report 1-sigma error bars, but one should state it. The authors should preferably report a 2-sigma error bar than state that they have a 96% CI, if the hypothesis of Normality of errors is not verified.
- For asymmetric distributions, the authors should be careful not to show in tables or figures symmetric error bars that would yield results that are out of range (e.g., negative error rates).
- If error bars are reported in tables or plots, the authors should explain in the text how they were calculated and reference the corresponding figures or tables in the text.

8. Experiments compute resources

Question: For each experiment, does the paper provide sufficient information on the computer resources (type of compute workers, memory, time of execution) needed to reproduce the experiments?

Answer: [Yes]

Justification: Compute resources and computational cost are reported in Appendix C.

Guidelines:

- The answer [N/A] means that the paper does not include experiments.
- The paper should indicate the type of compute workers CPU or GPU, internal cluster, or cloud provider, including relevant memory and storage.
- The paper should provide the amount of compute required for each of the individual experimental runs as well as estimate the total compute.
- The paper should disclose whether the full research project required more compute than the experiments reported in the paper (e.g., preliminary or failed experiments that didn't make it into the paper).

9. Code of ethics

Question: Does the research conducted in the paper conform, in every respect, with the NeurIPS Code of Ethics [https://neurips.cc/public/EthicsGuidelines?](https://neurips.cc/public/EthicsGuidelines)

Answer: [Yes]

Justification: The work uses simulated and controlled benchmark data and follows the NeurIPS Code of Ethics.

Guidelines:

- The answer [N/A] means that the authors have not reviewed the NeurIPS Code of Ethics.
- If the authors answer [No], they should explain the special circumstances that require a deviation from the Code of Ethics.
- The authors should make sure to preserve anonymity (e.g., if there is a special consideration due to laws or regulations in their jurisdiction).

10. Broader impacts

Question: Does the paper discuss both potential positive societal impacts and negative societal impacts of the work performed?

Answer: [N/A]

Justification: This is a technical work on misspecified SBI and does not have a direct broader societal impact.

Guidelines:

- The answer [N/A] means that there is no societal impact of the work performed.
- If the authors answer [N/A] or [No], they should explain why their work has no societal impact or why the paper does not address societal impact.

- Examples of negative societal impacts include potential malicious or unintended uses (e.g., disinformation, generating fake profiles, surveillance), fairness considerations (e.g., deployment of technologies that could make decisions that unfairly impact specific groups), privacy considerations, and security considerations.
- The conference expects that many papers will be foundational research and not tied to particular applications, let alone deployments. However, if there is a direct path to any negative applications, the authors should point it out. For example, it is legitimate to point out that an improvement in the quality of generative models could be used to generate Deepfakes for disinformation. On the other hand, it is not needed to point out that a generic algorithm for optimizing neural networks could enable people to train models that generate Deepfakes faster.
- The authors should consider possible harms that could arise when the technology is being used as intended and functioning correctly, harms that could arise when the technology is being used as intended but gives incorrect results, and harms following from (intentional or unintentional) misuse of the technology.
- If there are negative societal impacts, the authors could also discuss possible mitigation strategies (e.g., gated release of models, providing defenses in addition to attacks, mechanisms for monitoring misuse, mechanisms to monitor how a system learns from feedback over time, improving the efficiency and accessibility of ML).

11. Safeguards

Question: Does the paper describe safeguards that have been put in place for responsible release of data or models that have a high risk for misuse (e.g., pre-trained language models, image generators, or scraped datasets)?

Answer: [N/A]

Justification: The paper does not release high-risk models or datasets requiring special safeguards.

Guidelines:

- The answer [N/A] means that the paper poses no such risks.
- Released models that have a high risk for misuse or dual-use should be released with necessary safeguards to allow for controlled use of the model, for example by requiring that users adhere to usage guidelines or restrictions to access the model or implementing safety filters.
- Datasets that have been scraped from the Internet could pose safety risks. The authors should describe how they avoided releasing unsafe images.
- We recognize that providing effective safeguards is challenging, and many papers do not require this, but we encourage authors to take this into account and make a best faith effort.

12. Licenses for existing assets

Question: Are the creators or original owners of assets (e.g., code, data, models), used in the paper, properly credited and are the license and terms of use explicitly mentioned and properly respected?

Answer: [Yes]

Justification: We use standard open-source Python libraries, including PyTorch, NumPy, scikit-learn, and zuko, under their respective open-source licenses. We use the Causal Chambers datasets and mechanistic models for the controlled physical benchmarks and cite the original source. We do not redistribute or modify third-party datasets, pre-trained models, or code, and all licenses and terms of use are respected.

Guidelines:

- The answer [N/A] means that the paper does not use existing assets.
- The authors should cite the original paper that produced the code package or dataset.
- The authors should state which version of the asset is used and, if possible, include a URL.
- The name of the license (e.g., CC-BY 4.0) should be included for each asset.

- For scraped data from a particular source (e.g., website), the copyright and terms of service of that source should be provided.
- If assets are released, the license, copyright information, and terms of use in the package should be provided. For popular datasets, paperswithcode.com/datasets has curated licenses for some datasets. Their licensing guide can help determine the license of a dataset.
- For existing datasets that are re-packaged, both the original license and the license of the derived asset (if it has changed) should be provided.
- If this information is not available online, the authors are encouraged to reach out to the asset's creators.

13. **New assets**

Question: Are new assets introduced in the paper well documented and is the documentation provided alongside the assets?

Answer: [N/A]

Justification: The paper does not introduce a new dataset, model, or standalone released asset.

Guidelines:

- The answer [N/A] means that the paper does not release new assets.
- Researchers should communicate the details of the dataset/code/model as part of their submissions via structured templates. This includes details about training, license, limitations, etc.
- The paper should discuss whether and how consent was obtained from people whose asset is used.
- At submission time, remember to anonymize your assets (if applicable). You can either create an anonymized URL or include an anonymized zip file.

14. **Crowdsourcing and research with human subjects**

Question: For crowdsourcing experiments and research with human subjects, does the paper include the full text of instructions given to participants and screenshots, if applicable, as well as details about compensation (if any)?

Answer: [N/A]

Justification: The work does not involve crowdsourcing or human-subject experiments.

Guidelines:

- The answer [N/A] means that the paper does not involve crowdsourcing nor research with human subjects.
- Including this information in the supplemental material is fine, but if the main contribution of the paper involves human subjects, then as much detail as possible should be included in the main paper.
- According to the NeurIPS Code of Ethics, workers involved in data collection, curation, or other labor should be paid at least the minimum wage in the country of the data collector.

15. **Institutional review board (IRB) approvals or equivalent for research with human subjects**

Question: Does the paper describe potential risks incurred by study participants, whether such risks were disclosed to the subjects, and whether Institutional Review Board (IRB) approvals (or an equivalent approval/review based on the requirements of your country or institution) were obtained?

Answer: [N/A]

Justification: The work does not involve human-subject research.

Guidelines:

- The answer [N/A] means that the paper does not involve crowdsourcing nor research with human subjects.

- Depending on the country in which research is conducted, IRB approval (or equivalent) may be required for any human subjects research. If you obtained IRB approval, you should clearly state this in the paper.
- We recognize that the procedures for this may vary significantly between institutions and locations, and we expect authors to adhere to the NeurIPS Code of Ethics and the guidelines for their institution.
- For initial submissions, do not include any information that would break anonymity (if applicable), such as the institution conducting the review.

16. Declaration of LLM usage

Question: Does the paper describe the usage of LLMs if it is an important, original, or non-standard component of the core methods in this research? Note that if the LLM is used only for writing, editing, or formatting purposes and does *not* impact the core methodology, scientific rigor, or originality of the research, declaration is not required.

Answer: [N/A]

Justification: LLMs are not used as a core component of the method or experiments.

Guidelines:

- The answer [N/A] means that the core method development in this research does not involve LLMs as any important, original, or non-standard components.
- Please refer to our LLM policy in the NeurIPS handbook for what should or should not be described.